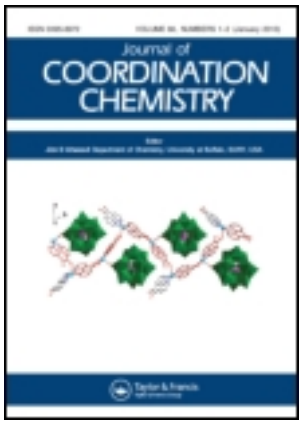

Journal of Coordination Chemistry
Publication details, including instructions for authors and subscription information:
http://www.tandfonline.com/loi/gcoo20

Crystal structures and physical properties of 5-sulfosalicylate and violurate metal-organic crystals - experimental versus theoretical study

Jüergen Storp [a], Cornelia Stolle [a], Bojidarka B. Ivanova [a] & Michael Spiteller [a]
[a] Institute of Environmental Research, Dortmund University, Otto-Hahn-Str. 6, D-44221 Dortmund, Germany
Accepted author version posted online: 03 May 2012.Published online: 15 May 2012.

To cite this article: Jüergen Storp, Cornelia Stolle, Bojidarka B. Ivanova & Michael Spiteller (2012) Crystal structures and physical properties of 5-sulfosalicylate and violurate metal-organic crystals - experimental versus theoretical study, Journal of Coordination Chemistry, 65:12, 2055-2073, DOI: 10.1080/00958972.2012.689294

To link to this article: http://dx.doi.org/10.1080/00958972.2012.689294

Journal of Coordination Chemistry
Vol. 65, No. 12, 20 June 2012, 2055–2073

Crystal structures and physical properties of 5-sulfosalicylate and violurate metal–organic crystals – experimental *versus* theoretical study

JÜERGEN STORP, CORNELIA STOLLE, BOJIDARKA B. IVANOVA* and MICHAEL SPITELLER

Institute of Environmental Research, Dortmund University, Otto-Hahn-Str. 6, D-44221 Dortmund, Germany

(*Received 3 October 2011; in final form 14 March 2012*)

Crystal structures, theoretical, and experimental physical properties of six coordination compounds of violuric and 5-sulfosalicylic acid (5SSA) with silver and potassium ions (**1**–**6**) are reported. The correlation between crystallographic data of the potassium violurate methanol solvate (**2**), potassium 5-sulfosalicylicilate salts (**3** and **4**), the redetermined structure for the potassium violurate dihydrate (**1**), and the already reported complexes of silver(I) with 5SSA (**5** and **6**) as well as the optical properties in the condensed phase was performed using the electronic-absorption, diffuse reflectance and fluorescence spectroscopies. The vibration characteristics of the crystals were studied by solid-state Raman spectroscopy. Special attention is focused on elucidation of the specific excitation phenomena within the THz-region, allowing unambiguously defining of the metal–organic polymorphs. The physical behavior and related processes under soft electrospray ionization (ESI) and matrix-assisted laser desorption/ionization (MALDI) mass spectrometric conditions are elucidated by corresponding methods, including imaging mass spectrometry (MS). A discussion on the stabilization of complex species and adducts in the gas phase depending on the type of metal ion was performed, with a view to their further application as matrices in the MALDI-Orbitrap MS method. The thermal properties were elucidated using the thermogravimetric and differential scanning calorimetric methods. Quantum chemical DFT calculations of the optical properties and selected thermodynamic quantities in solid-state were performed, supporting and elucidating some of the observed phenomena.

Keywords: Metal–organic crystals; 5-Sulfosalicylates; Violurates; Optical properties; Quantum chemistry; Mass spectrometry

1. Introduction

Remarkable progress has been made in coordination chemistry [1, 2], owing to their fascinating structural diversities and potential applications, such as magnetism, host-guest chemistry, catalysis, non-linear-optical, and functional porous materials [3, 4]. Non-covalent interactions, such as hydrogen bonding and π–π stacking, also greatly affect structures of the complexes [5], linking low-dimensional entities into

*Corresponding author. Email: B.Ivanova@infu.uni-dortmund.de; B.Ivanova@web.de

Journal of Coordination Chemistry
ISSN 0095-8972 print/ISSN 1029-0389 online © 2012 Taylor & Francis
http://dx.doi.org/10.1080/00958972.2012.689294

high-dimensional supramolecular networks [6]. 5-Sulfosalicylic acid (5SSA) has three potential coordinating centers, i.e. –OH, $–CO_2H$, and $–SO_3H$, allowing a large number of different coordination modes, depending on the reaction conditions [1–6]. Additionally, 5SSA and its derivatives have optical potency, not only in solution, but also in the solid state, making it a promising template for tuning of physical–optical properties in the condensed phase [6, 7]. Proton donating and accepting ability facilitate the modeling of hydrogen-bonding networks in the crystals to generate materials with non-centrosymmetric structures, thus leading to unique physical properties [8]. Similar to 5SSA, violuric acid (VA) was attractive as a ligand, for its tunable crystal packing, targeted design of the hydrogen bonding interactions, and coordination modes. The optical transmission properties of the corresponding derivatives are limited to within 500–1100 nm due to their self-absorption properties [8]. That is why we focus on the design of crystals with 5SSA and VA, containing more than one functional group, and self-absorption with potassium and silver ions. In parallel with the excellent coordination and/or protonation ability, the new crystals are characterized with a number of optical phenomena, both associated with the electronic transitions in the condensed phase as well as specific frequencies within the THz-region of the electromagnetic spectrum, good optical qualities, and reasonable rate of crystal growth as well as high thermal stability. In this article we discuss parallels between six crystals (figure 1) containing VA and 5SSA anions with the examination of their crystallographic X-ray diffraction structures, UV-VIS-NIR, *D*s, and *F*s spectra in the condensed phase, Raman frequencies, and mass spectrometric characteristics using the electrospray ionization (ESI) and matrix-assisted laser desorption/ionization (MALDI) Orbitrap imaging MS. Several theoretical density functional theory (DFT) approaches are correlated, tested and used to explain complex phenomena in the condensed phase. Despite the large number of studies of electronic transitions and related optical phenomena of both the acids and their metal complexes [9], studies of vibration characteristics within the THz-region and the properties of 5SSA derivatives as potential matrices for MALDI-MSI are rare [8]. The wide application of polyfunctional carboxylic acids as matrices in MALDI-MSI, typical soft ionization conditions stable in the gas-phase metal–organic species, as well as, the fact that potassium and sodium are essential constituents in all

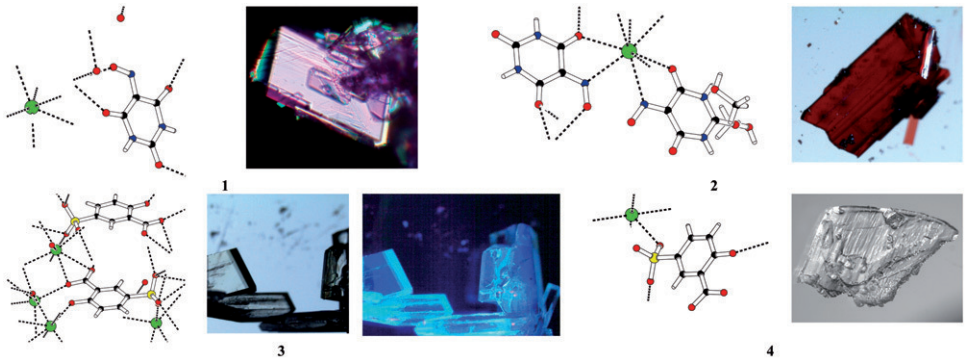

Figure 1. PLUTON diagrams of crystals of potassium violurate dihydrate (**1**), potassium violurate methanol solvate (**2**), potassium 5-sulfosalicylicilate salts (**3**), and Photographs of the crystals without and with irradiation at $\lambda_{ex} = 365$ nm (**4**).

biological organisms, make study of these important. Adducts with analyte samples are often observed in mass spectra due to performed parallel mass spectrometric ESI and the MALDI-MSI analysis of complexes of transition and alkali metal ions.

2. Experimental

2.1. *Physical measurements*

X-ray diffraction intensities were measured on a Bruker Smart X2S diffractometer using micro-source Mo-Kα radiation and employing the ω scan mode [10]. The structures in figure 1 are presented by PLATON. An absorption correction was based on multiple scanned reflections. The crystal structures were solved by direct methods using SHELXS-97 and refined by full-matrix least-squares refinement against F^2. Anisotropic displacement parameters were introduced for all non-hydrogen atoms. The hydrogen atoms attached to carbon were placed at calculated positions and refined allowing them to ride on the parent carbon. The experimental data are summarized in table 1. The obtained high R_1-factor of **4** was related to crystallographic disorder of the metal ion. The crystallographic refinement needed further comments according to the checkcif reported as achieved, using the International Union of Crystallography service (http://checkcif.iucr.org/), respectively. The alert level A PLAT780 (Type-1 "Test whether coordinates form a connected set") was a common error when dealing with isolated solvent oxygen, as water in the crystals of **3** and **4**, as solved (PLAT004 alert C, Type-5 Report "Dimensionality of polymer"). The alert level B PLAT774 (Type-1 "For too large/erroneous bond distance") in **2**–**4** were related to the crystallographic solution, suspecting a K^+–K^+ bond; from chemical point of view, however, covalent binding between these ions was unjustified. Same is valid for the level C alert suspecting

Table 1. Crystallographic and refinement data for **2**–**4**.

	2	**3**	**4**
Empirical formula	$C_{20}H_{25}N_{12}O_{20}K_2$	$C_{14}H_6K_4O_{15}S_2$	$C_{14}H_6O_{15}S_2K_4$
Formula weight	415.36	634.72	452.50
Temperature (K)	198(2)	204(2)	198(2)
Wavelength (Å)	0.71073	0.71073	0.71073
Crystal system	Triclinic	Monoclinic	Monoclinic
Space group	$P\bar{1}$	$P2_1/c$	$P2_1/c$
Unit cell dimensions (Å, °)			
a	6.444(3)	7.4067(15)	19.856(4)
b	7.527(3)	11.291(3)	5.4898(10)
c	17.570(8)	27.061(6)	18.814(4)
α	90.391(14)	90	90
β	99.196(14)	97.024(7)	103.984(6)
γ	97.017(14)	90	90
Volume (Å^3), Z	834.7(6), 1	2246.0(9), 4	1990.1(7), 4
Calculated density (Mg m^{-3})	1.655	1.877	1.881
Absorption coefficient (mm^{-1})	0.387	1.054	0.965
Crystal size (mm^3)	0.41 × 0.28 × 0.21	0.14 × 0.07 × 0.05	0.63 × 0.22 × 0.16
Goodness-of-fit on F^2	1.089	1.088	1.496
R_1 [$I > 2\sigma(I)$]	0.0587	0.0708	0.0908

X–*Y* bonding between the K^+ and O^-/S atoms, because of the strong ionic character typical for these interactions in the crystals of K^+ salts. In addition to crystallographic phenomena, defects in the crystals of this compound (figure 1) also resulted in the obtained high value. The UV-VIS-NIR spectra between 190 and 1190 nm, using acetonitrile (Uvasol, Merck product) at a concentration of $2.5 \cdot 10^{-5}$ mol L^{-1} in 0.921 cm quartz cells, were recorded on a Tecan Safire Absorbance/Fluorescence XFluor 4 V 4.40 spectrophotometer. The thermogravimetric study was carried out using a Perkin-Elmer TGS2 instrument. Calorimetric measurements were performed on a DSC-2C Perkin-Elmer apparatus under argon. Solid-state UV-Vis spectra were measured on a Perkin-Elmer Lambda 750 in reflectance mode. The reflection spectra were automatically converted to absorbance spectra using the Kubelka–Munk theory. HPLC-MS/MS measurements were made using a TSQ 7000 instrument (Thermo Electron Corporation). Two mobile phase compositions were used: (A) 0.1% v/v aqueous HCOOH and (B) 0.1% v/v HCOOH in CH_3CN. ESI mass spectrometry (MS) used a triple quadrupole mass spectrometer (TSQ 7000 Thermo Electron, Dreieich, Germany) equipped with an ESI 2 source operating at the following conditions: capillary temperature 180°C; sheath gas 60 psi, corona 4.5 µA, and spray voltage 4.5 kV. Sample was dissolved in acetonitrile (1 mg mL^{-1}) and was injected in the ion source by an autosampler (Surveyor) with a flow of pure acetonitrile (0.2 mL min^{-1}). Data processing was performed by Excalibur 1.4 software. A standard LTQ Orbitrap XL instrument is used for all the experimental work described in this article. An overall mass range of *m*/*z* 100–1000 is scanned simultaneously in the Orbitrap analyzer. The samples were measured in the solid-state, using a variant of the spray technique of solution, containing the matrix and analyte compound. The solution of thin liquid films is rapidly evaporated to form the sample of matrix/matrix/analyte. Conventional infrared (IR) and Raman spectroscopy in solid state were performed on a Thermo Nicolet 6700 FTIR spectrometer (4000–400 cm^{-1}, resolution 0.5 cm^{-1}, and 100 scans) and a NXR FT-Raman module from 4000 cm^{-1} to 50 cm^{-1}. The content of metal ions are obtained by the ICP measurements on the ICP–OES Thermo Elemental spectrometer with atomisator Argon plasma. They are detected by following the lines for Ag (328.0 and 338.2 nm). The analyses of the samples by ESI-MS were performed with a Thermo Finnigan surveyor LC-Pump. Compounds were separated on a Luna C18 column (150 × 2 mm, 4 µm particle size) from Phenomenex (Torrance, CA, USA) using a gradient program.

2.2. *Quantum chemical calculations*

Quantum chemical calculations are performed with GAUSSIAN 09 and Dalton 2.0 program packages, visualizing by the GausView03 program package [11]. The geometries were optimized by DFT employing B3LYP, CAM-B3PW91, and M06-2X functionals. Molecular geometries of the studied species were fully optimized by the force gradient method using Bernys' algorithm. For every structure, the stationary points found on the molecule potential energy hypersurfaces were characterized using standard analytical harmonic vibrational analysis. The absence of imaginary frequencies, as well as of negative eigenvalues of the second-derivative matrix, confirmed that the stationary points correspond to minima of the potential energy hypersurfaces. The calculation of vibrational frequencies and IR intensities were checked to establish which

calculations agree best with the experimental data. The electronic-absorption and fluorescence spectra in the gas phase and methanol are detected by TDDFT calculations. We have utilized primarily the polarizable continuum model. The calculations are utilized by the triple-ζ quality TZVP, triple-ζ plus double polarization TZ2P, Los Alamos National Laboratory's 2 double-ζ as well as quasirelativistic effective core pseudopotentials from the Stuttgart–Dresden method. The large "correlation consistent" basis sets aug-cc-pVDZ and aug-cc-pVTZ (augmented correlation-consistent polarized valence double and triple zeta levels) are also applied in few cases.

2.3. *Statistical approaches*

The experimental and theoretical spectroscopic patterns were processed by R4Cal OpenOffice STATISTICs for Windows 7 program package [12]. Baseline corrections, linear and non-linear curve-fitting procedures were applied. The mixed non-linear function of the Gauss type best fits to the experimental data set, giving r^2 values shown in figure 2. The deviations of the highest r^2 value of 0.9985_4–0.9982_7 are discussed. The statistical significance of each regression coefficient was checked by the use of *t*-test. The model fit was determined by *F*-test (comparison of calculated by the model and experimentally obtained signal values). Details are given in [12].

2.4. *Synthesis*

Crystals of **1**–**4** were obtained by mixing VA (0.074 g, Sigma) or 5SSA (0.173 g, Sigma-Aldrich) acids in a solvent mixture of methanol : water 1 : 1 with 10 mL of 1 mol L^{-1} KOH. The resulting crystals (figure 1) were filtered off, washed with CH_3OH, and dried over P_2O_5 at 298 K. The synthesis of **5** and **6** are as reported [1h]. To a mixture of 5SSA (0.11 g) and NaOH (0.040 g) in water (5 mL), a solution of $AgNO_3$ (0.170 g) in water (10 mL) was added under stirring for 30 min. Colorless crystals of **5** were obtained after the filtrate was left at room temperature. Calcd for $C_7H_6Ag_2O_7S$: C, 18.7; H, 1.3; found: C, 18.3; H, 1.2. To a solution of the same acid (0.22 g) and MgO (0.020 g) in water (5 mL), a solution of $AgNO_3$ (0.170 g) in water was added. Colorless crystals of **6** were obtained when the filtrate was left at room temperature. Calcd for $C_{14}H_{18}Ag_2O_{16}S_2$: C, 23.3; H, 2.5; found: C, 22.7; H, 2.3. The single-crystal X-ray diffraction *hkl* collection confirmed the reported data. TGV and DSC data from 300 to 500 K confirmed the crystallographic amounts for solvent included in the reported structures. The obtained dependences of **2**, **5**, and **6**, which are discussed (below) are interesting.

3. Results and discussion

3.1. *Crystallographic data*

Compounds **1** and **2** are potassium salts of VA, crystallizing in the $P2_1/c$ and $P\bar{1}$ space groups (figure 1). The structure of **1** is a redetermination of the already reported potassium violurate dihydrate [9], while **2** is the methanol solvate derivative. Seven- and

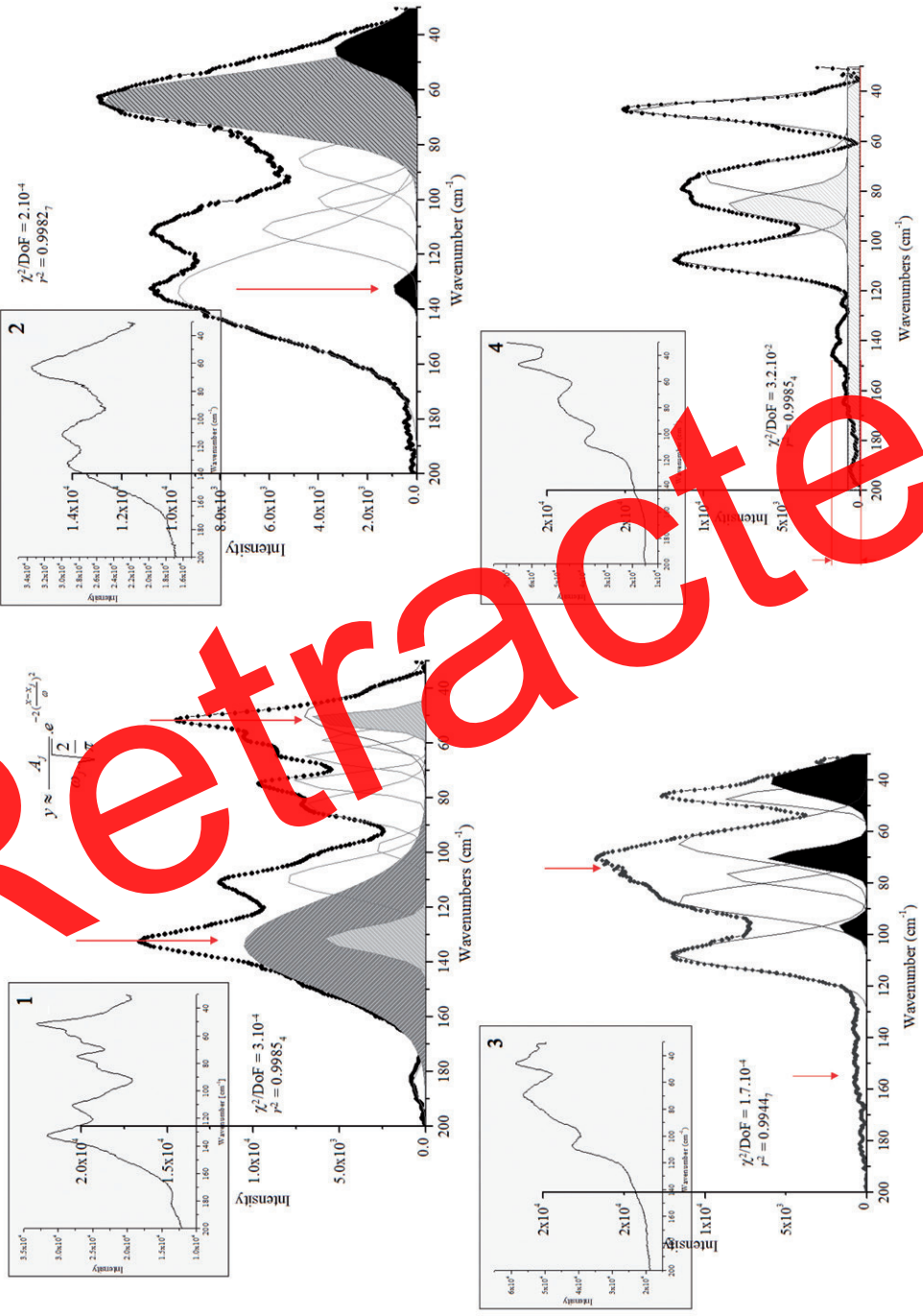

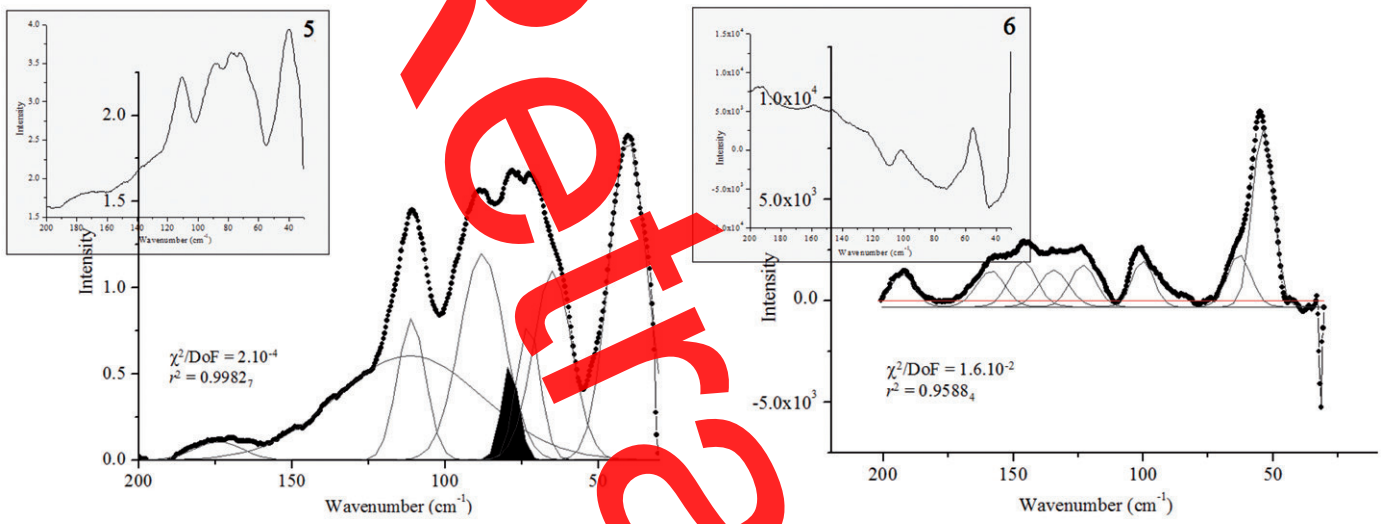

Figure 2. Experimental solid-state Raman spectra of **1**–**6** within 200–30 cm^{-1} (small figures); experimental patterns with baseline correction and non-linear curve-fit after the applied deconvolution; corresponding r^2 and (χ^2/DoF) statistical values.

eightfold coordination of potassium cation is observed in **1** and **2**, respectively. The $K^+ \cdots O$ distances in **1** are 2.737–2.892 Å, while for **2** are 2.753–2.864 Å ($K^+ \cdots O$), 2.910 and 2.959 Å ($K^+ \cdots N$). The theoretical triprotic proton-donation, i.e. by $-SO_3H$, –COOH, and –OH, characterizing 5SSA with $K_1 > 0.1$, $K_2 = 1.4.10^{-3}$, and $K_3 = 4.10^{-14}$ values, is evaluated experimentally. In the presence of strong basic media such as for obtaining crystals of **3** and **4**, 5SSA is a diprotic acid. Compound **3**, $P2_1/c$ space group, contains eightfold coordinated potassium with $K^+ \cdots O$ distances of 2.671–3.301 Å (figure 1). In contrast to **3**, the second isolated potassium salt of 5SSA, **4**, also has $P2_1/c$ space group, six coordination of potassium with $K^+ \cdots O$ distances of 2.679–2.855 Å (figure 1). Compound **5** has one type of $5SSA^{2-}$ in the structure, where each sulfonate binds to five different Ag^I ions, with two oxygen atoms each binding to two different silver ions, while the remaining oxygen binds to a single silver. As has been reported [1], this is a highly unusual coordination mode for an $R\text{-}SO_3^-$ [1, 8]. Each COO^- is a bridging ligand to join two silver ions. Each hydroxyl is coordinated to one silver ion. The Ag–Ag distance is 2.78 Å. In **6** $-SO_3H$ is deprotonated, but –OH groups and $-CO_2H$ are neutral. There are two kinds of crystallographically unique $5SSA^-$ anions in the structure, and both show a similar coordination mode (figure 1). Each sulfonate binds to three different silver ions, with one oxygen binding two different silver ions, while one oxygen binds to only a single silver, and the third oxygen does not coordinate to silver. Each $-CO_2H$ coordinates to one silver, although neutral $-CO_2H$ is a weakly coordinating group; the hydroxyl is not coordinated to silver. Our quantum chemical calculations of the optical properties of **1**–**6** are performed using the crystallographic unit cell contents and the asymmetric units, according to the described methods [8]. The obtained data for fluorescence of **5** and **6** are compared with the experimental ones [1].

3.2. *Electronic absorption, diffuse reflectance, and fluorescence data in condensed phase*

The observed absorption bands in the metal–organic violurate crystals (**1** and **2**) from 500 to 665 nm limits wide application of these derivatives as NLO materials. The violurate co-crystals and corresponding barbiturates have transmission properties within 390/400–1100 nm range [8], while electronic spectra of 5SSA derivatives with stabilizing cations have a "transmission window" from 290 nm to 1100 nm. The 5SSA derivatives have bands at 200, 230, and 290 nm (ε_ν of 16000, 15000, and 4000 $L\,mol^{-1}\,cm^{-1}$). Deprotonation of $-SO_3H$ weakly affects λ_{max} of K- and B-bands as well as the $n \rightarrow \pi^*$ transition. The MO6-2X XC has good agreement with the electronic transitions in these systems (table 2). Moreover, the predicted higher f values of the studied systems by the first two functionals correlate better to the experimental ε_ν. The HOMO–LUMO gaps (scheme 1) suggest open-shell singlet ground state as well as stabilization and charge redistribution within the frame of the molecular crystals (see, e.g., scheme 1).

For all systems a solid-state emission ~350–400 nm for **3** and **4**, similar to **5** and **6** [1], enhance $\pi \rightarrow \pi^*$ transitions in ES (see, e.g., figures 2 and 3). Our calculations of the molecular species (scheme 1) show the expected series of fluorescence bands for the cations [8]. Additional confirmation follows from our study of the corresponding electronic transitions in the crystals, thus evaluating the possible interlayer CT effect

Table 2. Theoretical and experimental values of λ_{max} for electronic transitions in crystals of **1**–**6**.

λ_{max}											
1		**2**		**3**		**4**		**5**		**6**	
Theor.	Exp.	Theor.	Exp.	Theor.	Exp.	Theor.	Exp.	Theor.	Exp.	Theor.	Exp.
280	330	280	286	220	210	255	260	220	218	300	295
340	339	343	295	275	280	280	280	280	278		306
350	351	360	311	322	318	344	337	355	356	320	322
			329				348			346	340
			347								

within the frame of the molecules in the unit cells. The obtained data could explain the contribution of the number of sub-component multiple character of the bands in the DS spectra at 330–350 nm for **3**–**6**.

3.3. *Vibrational properties*

Solid-state IR-spectra of the complexes of 5SSA within the mid-IR region show low-intensity IR-bands at 1610 and 1578 cm^{-1} of the in-plane (i.p.) vibrations of the 5SSA skeleton (theoretical values of 1607 and 1575 cm^{-1}), which are weak effects of the deprotonation of $-SO_3H$ in the salts. The same consideration is valid for the corresponding o.p. γ_4 and γ_{11} at 715, 660, and 575 cm^{-1}. The typical asymmetric sub-fragment $-SO_3H$ IR-bands are $1415 \pm 85\ cm^{-1}$ ($\nu^{as}_{SO_2}$) and $1195 \pm 60\ cm^{-1}$ ($\nu^{as}_{SO_2}$). The ν_{S-O} is observed at $795 \pm 35\ cm^{-1}$. The vibrations of VA anions in the complexes depend on the hydrogen bonding scheme. IR-bands at 1780, 1760, and 1730 cm^{-1} [8] belonging to $\nu_{C=O} + \delta_{N-H}$ as well as those at 841 and 808 cm^{-1} of $\delta_{NH} + \delta_{CNOH} + \nu_{CCC}$ and $\rho_{CCC} + \rho_{NOH} + \rho_{NCN}$ modes, respectively, differ by 15–23 cm^{-1} depending on the interaction type in the crystals of **1** and **2**, respectively [8].

Raman spectra in the THz-region, however, are characteristic for determination of the chemical substance, according to recent studies [9]. The region of 6.0–0.9 THz show well-defined and intensive modes (table 3), belonging to the H-bonding deformations, lattice and skeletal vibrations, as well as coupling modes. Specific interactions in crystals of **1**–**6** result in strong individual patterns within the 200–30 cm^{-1} region, allowing their determination in the crystalline state (figure 3). Detailed analysis shows that molecular excitations within this region by the THz-spectroscopy, Raman or far-IR methods [9] allow determination of the polymorphs. In our case, examples are **3** and **4**. Group theoretical analysis predicts two components for internal modes in either the Raman or IR-spectrum; nine lattice modes, much closer to our experimental observation for the Raman spectra of **3** and **4**. In calculations of all four molecules, the number of expected optical lattice modes is 21, of which 12 are Raman- and 9 IR-active. The observed LO–TO splitting of the bands is illustrated by the application of curve-fitting and deconvolution procedures after preliminary baseline correction (figure 3) [8]. Application of the same procedures to spectroscopic patterns of the dyes (**2**) within 200–30 cm^{-1} reveals a series of maxima, where the number of observed Raman bands correlated well to the triclinic *P* space system. The correlation between

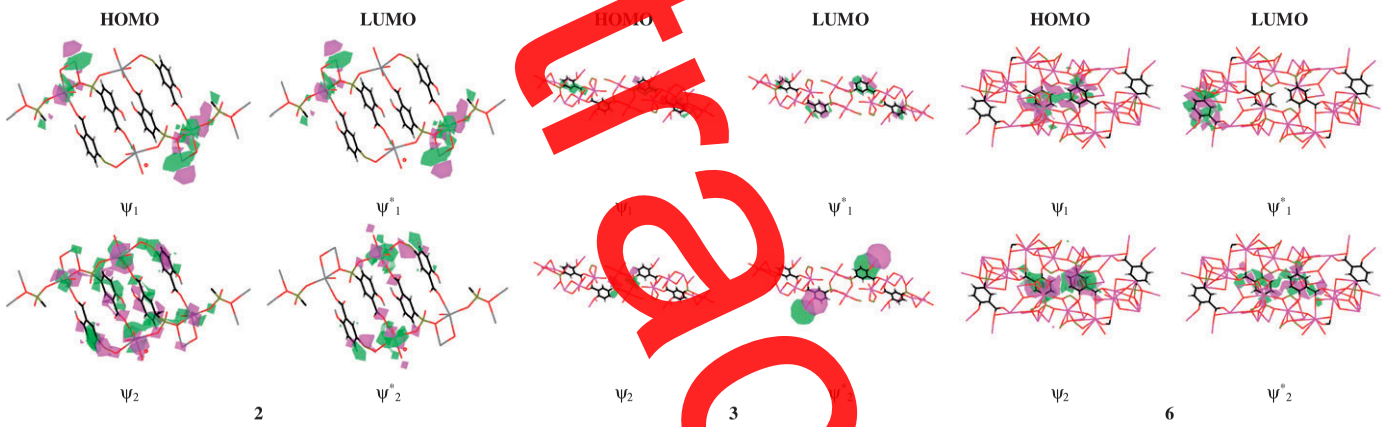

Scheme 1. HOMO–LUMO MO gaps of **2**, **3**, and **6**, respectively. The calculations are performed using the crystallographic input parameters and unit cell contents; the theoretical values of λ_{calc} are shown in table 2.

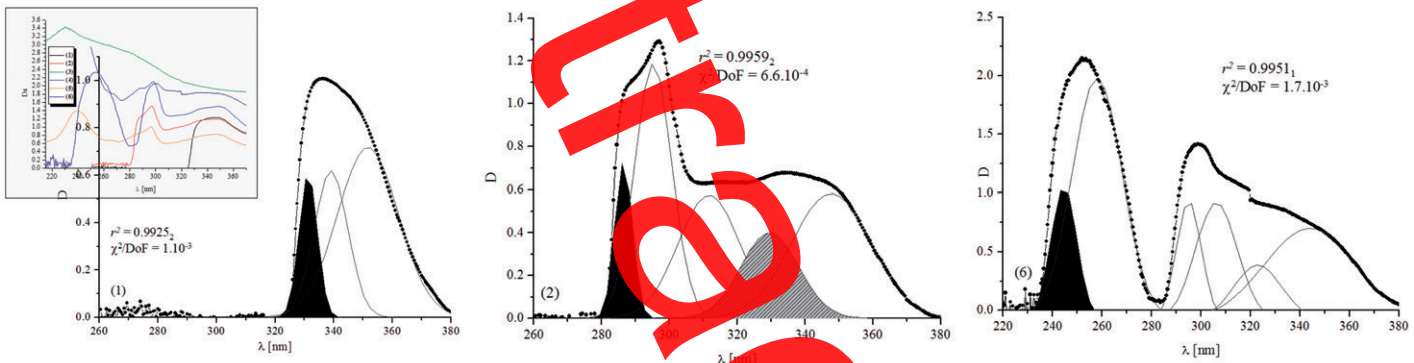

Figure 3. Experimental diffuse reflectance spectra (small figure) of **1**–**6**; corresponding spectroscopic patterns with the baseline correction method and non-linear curve-fitting; r^2 and (χ^2/DoF) statistical values.

Table 3. Solid-state Raman frequencies and assignment of **1**–**6** from 200–30 cm^{-1}; ν [cm^{-1} (THz)]; the theoretical data are obtained from calculations of the crystallographic input parameters and unit cell contents.

	1		**2**		**3**		**4**		**5**		**6**	
	Theor.	Exp.	Theor.	Exp.	Theor.	Exp.	Theor.	Exp.	Theor.	Exp.	Theor.	Exp.
											200 (6.0)	192 (5.7)
	190 (5.7)	184 (5.5)										
									180 (5.4)	174 (5.2)		
H-bonding			165 (4.9_5)	165 (4.9_5)			165 (4.9_5)	165 (4.9_5)			160 (4.8)	158 (4.7)
deformations											144 (4.3)	146 (4.3_8)
OH···OS, OH···O,	130 (3.9)	133 (3.9_9)	130 (3.9)	133 (3.9_9)							135 (4.1)	134 (4.0)
N^+H_3···O, N^+H_2···O											122 (3.6_6)	123 (3.6_9)
	110 (3.4_7)	109 (3.3)	110 (3.4_7)	110 (3.4_7)	109 (3.3)	107 (3.2)	105 (3.1)	106 (3.1)		111 (3.3)		
									110 (3.3)	110 (3.3)		
	100 (3.0)	98 (2.9)	100 (2.9)	100 (2.9)	95 (2.8_5)	97 (2.8)					100 (3.0)	100 (3.0)
Skeletal modes	**85 (2.5)**	**83 (2.4_9)**	**85 (2.5)**	**85 (2.5)**	**85 (2.5)**	**85 (2.5)**	**85 (2.5)**	**85 (2.5)**	80 (2.4)	87 (2.6)		
	77 (2.3)	74 (2.2)				77 (2.3)	75 (2.2_5)	74 (2.2)		78 (2.3)	80 (2.4)	79 (2.3_7)
					70 (2.1)	70 (2.1)			70 (2.1)	72 (2.1_6)		
	65 (1.9_5)	65 (1.9_5)	65 (1.9_5)	64 (1.9)	65 (1.9_5)	64 (1.9)			65 (1.9_5)	64 (1.9)	65 (1.9_5)	65 (1.9_5)
	60 (1.8)	58 (1.7)										
	50 (1.5)	51 (1.7)					55 (1.6_3)	56 (1.6_8)			55 (1.6_5)	54 (1.6)
Torsion of entire		49 (1.4_7)	44 (1.7_9)	45 (1.7_9)	45 (1.7_9)	46 (1.8)	45 (1.3_5)	47 (1.8)	40 (1.2)	40 (1.2)		
side chain						40 (1.2)						
about the								35 (1.0_5)				
aromatic system							30 (0.9)		30 (0.9)	31 (0.9)		

the theoretical and experimental Raman spectra in the same region calculated for the unit cell contents show the applicability of the theoretical approach for the prediction of molecular motions within the ensemble of interacting species. The differences *ca* 3–4 cm^{-1} for the predicted positions of the frequencies assigned to H-bonding deformations (within 200–100 cm^{-1}) could be associated to the following possible sources of the errors: (a) errors from the applied theoretical methods. In this case, however, the differences of the predicted vibrations for the skeletal modes are less than 1 cm^{-1}, indicating that the errors of the theoretical methods are negligible for these calculations. (b) Errors from the applied mathematical methods for the interpretation of experimental spectroscopic patterns. In these cases, it is important to note that the r^2 values are affected strongly by the signal-to-noise ratio (see, e.g., figure 3) or artifacts such as overlapped peaks after deconvolution and curve-fitting procedures; (c) Errors from definition of proton positions by single-crystal X-ray diffraction. For skeletal modes, lattice vibrations in the systems are assigned to excitations within *ca* 100–50 cm^{-1}. The excitation about 70 cm^{-1} (table 3) is assigned to the CCαN deformations.

3.4. *Thermal properties*

TG/DSC analytical data for **2**, **5**, and **6** quantify weight loss at various temperatures with no overlap. The 9.2% weight loss at 142–150°C is solvent methanol. The larger loss of 10.7% at 300–418°C is attributed to the decomposition of **2**. Compound **6** shows weight loss, *ca* 127°C, associated to water joined as ligand to Ag^{I} (4.82%). The similar curve profile at 152–166°C in both **5** and **6** correspond to 10.39% for **5** and 11.44% for **6** weight loss within 142–150°C, associated with bridging water (figure 4). The obtained molar ratios of metal ion to ligand by ICP-AES are 2.7 : 1 for **5** and 1.3 : 1 for **6**, deviating from the theoretical values of 2 : 1 and 1 : 2 (see also the elemental analysis), which could be associated with the red-ox process Ag(I) → Ag(0) in the presence of NaOH. The DSC curves agree with TG data. An exothermal peak

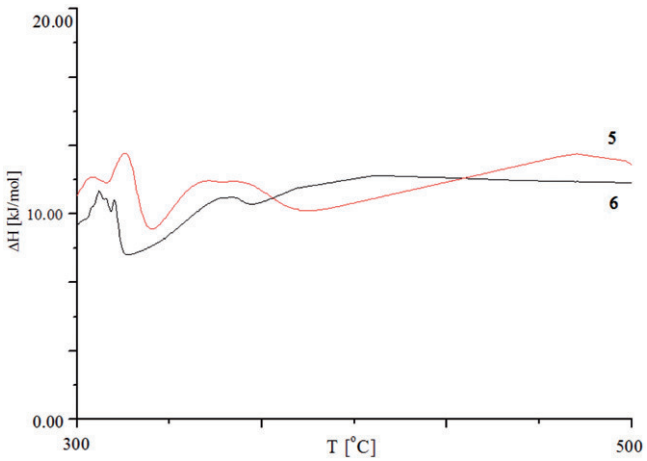

Figure 4. DSC data for **5** and **6**.

at 416–440°C appears in both complexes. The fine curve profile of weight loss below 150°C could be associated to adsorbed water on the silver metal surfaces [13]. The much higher temperature peaks over 450°C are associated with degradation of the complexes.

3.5. *Mass spectrometric data*

The use of polyfunctional carboxylic acids as matrices in MALDI imaging MS encourage detailed study of the behavior of **1**–**6** under ionization/desorption conditions [14]. According to the well-known techniques for solid-sample preparation the matrix-to-analyte ratio is *ca* 10^4 : 1. We evaluate the effect of the signals of **1**–**6** for potential use as metal–organic matrices. The MS analysis both by MALDI and ESI methods of potassium-free ions and ion/analyte adducts in the gas phase are of special interest, since alkali metal ions such as potassium and sodium are essential constituents in all biological organisms [15]. Adding in the MALDI matrix solution is attempted to circumvent this obstacle for small molecule analysis. The obtained data for **1**–**6** are depicted in figures 5 and 6. Results of the parallel study of transition metal complexes and complex salts of potassium are examined by the ESI-MS and MALDI-MSI methods. Any charged solution added at high concentration can compete with the analyte and cause signal suppression [14] in ESI-MS. In our case, the analyte appears as 5SSA anions stabilized as transition metal complexes or salts. Since the function of ESI is to transfer ions in solution to the gas phase, the results of figure 5 represent the ESI MS spectra of the highly concentrated ionic liquid at molar ratio of the metal-to-ligand proportional to the presented amounts in figure 1. Under these conditions the MS spectra of **5** and **6** show metal-to-ligand charge transfer complexes stable in the gas phase of the type described earlier [8]. Similar metal–organic species of silver(I) are found in corresponding MALDI-MSI spectra depicted in figure 6. The obtained ratios of metal ions, from observation of the peaks at *m/z* 141.0, correspond to the metal-to-ligand ratio 2 : 1 of the doubly charged complex $[C_3H_4N_2Ag_2]^{2+}$ (molecular weight of 283.54). The small intense signal for the cationic analyte 5SSA is observed at *m/z* 218.27. Regardless of the observable peaks for **5** and **6**, the obtained relatively small response could allow their application as matrices for MALDI-MSI, taking into account the possible competitive complex formation with analyte samples. The potassium salts of 5SSA show interesting dependences (figures 5 and 6). At low concentrations the ESI-MS data extrapolate with the relationships obtained previously [16]. The addition of smaller amount improves the ESI response, thus observing the peak at *m/z* 218.65 of the cationic acid and the corresponding K^+-adduct at *m/z* 256.17. If, however, we analyze the total amount of the complex salts used as matrix for MALDI-MSI in an ESI-MS experiment, the intensity of the signals drastically decrease (figure 5). This is also observed for the corresponding MALDI-MSI spectra (figure 6). Quantitative values show a higher decreasing effect, especially the signal for the K^+-adduct. The data indicate that the deprotonated matrix can reduce the number of free alkaline cations. In this respect the role of the $-SO_3H$ functional group is underlined [16a]. The strong acidic properties, including stabilizing of mono and dianions, of the 5SSA and the possibility for polydentate coordination make it suitable as matrix both in neutral as well as deprotonated ligand for MALDI-MSI measurements, especially in cases where suppression of the signals of ''obstacle'' metal ions and/or selective analysis is of interest.

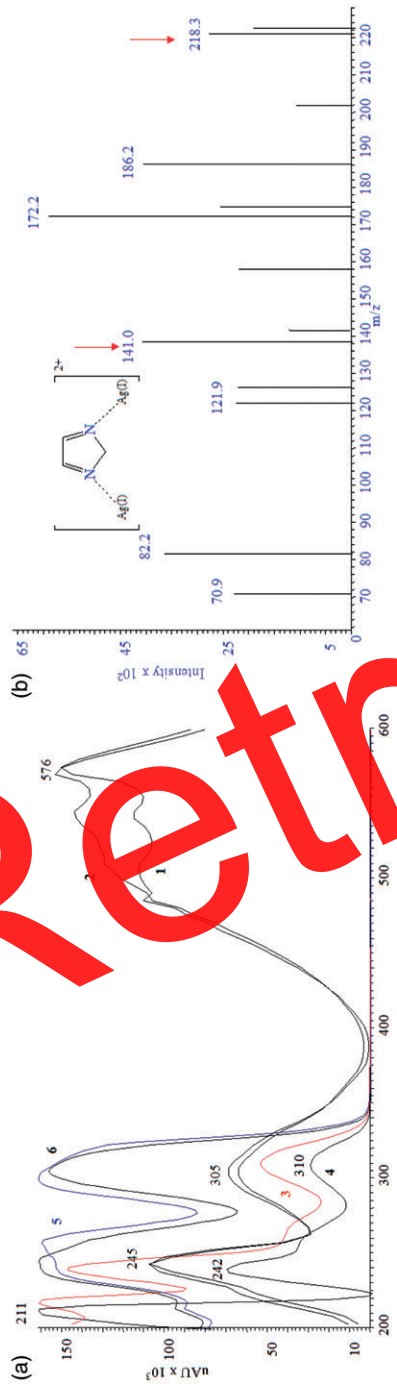

Figure 5. Electronic transitions of **1**–**6** (a); ESI-MS data of **1** (b) and **3** (c), respectively.

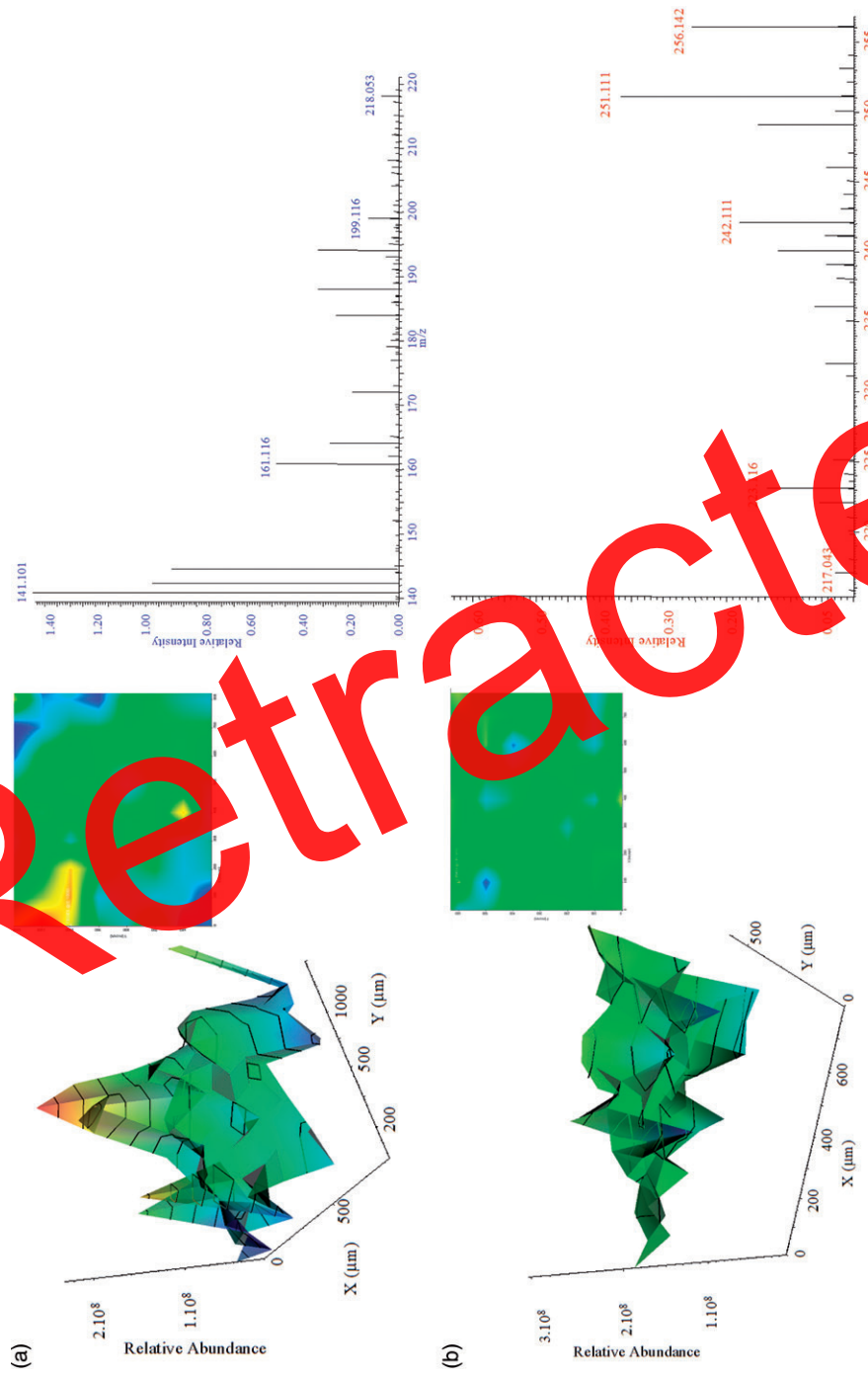

Figure 6. 3-D and 2-D image by logarithm plotting of Δx, Δy *vs.* the signal amplitude (grid) of selected ion range of **3** (a) and **5** (b), obtained by MALDI-MSI, using the Orbitrap analyzer; the corresponding mass spectra.

4. Conclusions

We have demonstrated an effect of 5-sulfosalicylate in metal–organic crystals of silver(I) and potassium complex salts on the physical properties, including the optical electronic transitions and phenomena within the UV-Vis and far-IR ranges of the spectrum, making a parallel between these and corresponding violurate derivatives. The key of our approach lies in the excellent correlation between theoretical properties and experimental crystallographic results of six crystallographic objects of analysis, allowing explanation of the observed complex optical phenomena in the diffuse reflectance, fluorescence, and Raman spectra. The important observation from this study is the correlation between ESI-MS and MALDI-MSI analysis of the complexes of silver(I) and corresponding potassium complex salts of 5SSA as possible metal–organic matrixes for MALDI-MSI. In both cases at high concentrations the matrix signals are suppressed, including the stable metal-to-ligand charge transfer complexes of silver(I) or K^+-adducts/free metal ions, in the second case. These data indicate that the strong acidic character of 5SSA and its polydentate coordination ability make it suitable as a deprotonated matrix ligand for MALDI-MSI experiments. Application of chelating further functionalized derivatives as organic matrices, in cases where suppression of the signals of the "obstacle" metal ions as well as selective analysis of the metal ions, is thus possible.

The "tuning" of the fragment ions by judicious choice of matrix requires additional studies with the functional analyte on the basis of 5SSA and/or related derivatives with polydentate coordination ability as ligands, as well as yields of transition metal complexes and/or complex salts that examine other aspects of matrix structure for detailed elucidation of the observed processes in MALDI.

Supplementary material

Crystallographic data for the structural analysis of **1**–**4** have been deposited with the Cambridge Crystallographic Data Centre, CCDC 782348–782351. Copies of this information may be obtained from the Director, CCDC, 12 Union Road, Cambridge, CB2 1EZ, UK (Fax: +44 1223 336 033; E-mail: deposit@ccdc.cam.ac.uk or http://www.ccdc.cam.ac.uk).

Acknowledgments

The authors thank the Deutscher Akademischer Austausch Dienst (DAAD), the Deutsche Forschungsgemeinschaft (DFG), the central instrumental laboratory clusters for structural analysis at University Dortmund (Germany) and the analytical and computational laboratories at the Institute of Environmental Research (INFU) at the same University.

References

[1] (a) D. Caulder, K. Raymond. *Acc. Chem. Res.*, **32**, 975 (1999); (b) P. Hagrman, D. Hagrman, J. Zubieta. *Angew. Chem. Int. Ed.*, **38**, 2638 (1999); (c) S. Batten, R. Robson. *Angew. Chem. Int. Ed.*, **37**, 1461 (1998); (d) L. Carlucci, G. Ciani, D. Proserpio. *Coord. Chem. Rev.*, **246**, 247 (2003); (e) R. Matsuda, R. Kitaura, S. Kitagawa, Y. Kubota, R. Belosludov, T. Kobayashi, H. Sakamoto, T. Chiba, M. Takata, Y. Kawazoe, Y. Mita. *Nature*, **436**, 238 (2005); (f) B. Ye, M. Tong, X. Chen. *Coord. Chem. Rev.*, **249**, 545 (2005); (g) Z. Lu, L. Wen, J. Yao, H. Zhu, Q. Meng. *CrystEngComm*, **8**, 847 (2006); (h) J. Ma, Y. Yang, S. Li, S. Song, H. Zhang, H. Wang, K. Yang. *Cryst. Growth Des.*, **5**, 807 (2005); (i) Z. Lu, L. Wen, Z. Ni, Y. Li, H. Zhu, Q. Meng. *Cryst. Growth Des.*, **7**, 268 (2007); (j) J. Ma, J. Li, G. Zheng, J. Liu. *Inorg. Chem. Commun.*, **6**, 581 (2003); (k) G. Shimizu, G. Enright, C. Ratcliffe, G. Rego, J. Reid, J. Ripmeester. *Chem. Mater.*, **10**, 3282 (1998); (l) G. Lawrance. *Chem. Rev.*, **86**, 17 (1986).

[2] (a) R. Robson, B. Abrahames, S. Batten, R. Gable, B. Hoskins, J. Liu. *Supramolecular Architecture*, Chap. 19, American Chemical Society, Washington DC (1992); (b) J. Lehn. *Supramolecular Chemistry: Concepts and Perspectives*, VCH, New York (1995); (c) G. Desiraju. *Crystal Design: Structure and Function, Perspectives in Supramolecular Chemistry*, Wiley, Chichester (2003).

[3] (a) K. Inoue, H. Imai, P. Ghalsasi, K. Kikuchi, M. Ohba, H. Okawa, J. Yakhmi. *Angew. Chem. Int. Ed.*, **40**, 4242 (2001); (b) K. Inoue, T. Hayamizu, H. Iwamura, D. Hashizume, Y. Ohashi. *J. Am. Chem. Soc.*, **118**, 1830 (1996); (c) M. Eddaoudi, D. Moler, H. Li, B. Chen, T. Reineke, M. O'Keeffe, O. Yaghi. *Acc. Chem. Res.*, **34**, 319 (2001); (d) S. Batten, K. Murray. *Coord. Chem. Rev.*, **246**, 103 (2003); (e) S. Kitagawa, R. Kitaura, S. Noro. *Angew. Chem. Int. Ed.*, **43**, 2334 (2004).

[4] (a) C. Janiak. *Dalton Trans.*, 2781 (2003); (b) C. Wu, W. Lin. *Angew. Chem. Int. Ed.*, **44**, 1958 (2005); (c) M. Zeng, W. Zhang, X. Sun, X. Chen. *Angew. Chem. Int. Ed.*, **44**, 3079 (2005); (d) J. Zhang, Y. Lin, X. Huang, X. Ren. *J. Am. Chem. Soc.*, **127**, 5495 (2005).

[5] (a) S. Kitagawa, K. Vemura. *Chem. Soc. Rev.*, **34**, 109 (2005); (b) J. Zhang, Y. Wang, X. Huang, Y. Lin, X. Ren. *Chem. Eur. J.*, **11**, 552 (2005); (c) M. Fujita. *Acc. Chem. Res.*, **32**, 53 (1999); (d) D. Amabilino, J. Stoddart. *Chem. Rev.*, **95**, 2725 (1995); (e) K. Park, D. Wang, E. Lee, J. Heo, K. Kim. *Chem. Eur. J.*, **8**, 498 (2002); (f) Y. Li, L. Deng, X. Zhou, S. Zhang. *Acta Phys. Chim. Sin.*, **14**, 778 (1998).

[6] (a) C. Liu, X. Shi, J. Li, J. Wang, X. Bu. *Cryst. Growth Des.*, **6**, 656 (2006); (b) Y. Wan, L. Zhang, L. Jin, S. Gao, S. Lu. *Inorg. Chem.*, **42**, 4985 (2006); (c) G. Whitesides, J. Mathias, C. Seto. *Science*, **254**, 1312 (1991); (d) B. Moulton, M. Zaworotko. *Chem. Rev.*, **101**, 1629 (2001).

[7] (a) G. Smith, U. Wermuth, J. White. *Acta Cryst.*, **61C,** o105 (2005); (b) G. Smith, U. Wermuth, J. White. *Acta Cryst.*, **61E,** o213 (2005); (c) G. Wu, X. Wang, X. Guo, L. Yu. *Z. Anorg. Allg. Chem.*, **636**, 652 (2010).

[8] (a) C. Bosshard, J. Hulliger, M. Florsheimer, P. Günter. *Organic Nonlinear Optical Materials, Advances in Nonlinear Optics*, Gordon and Breach Sci. Publishers S.A., Postfach, Basel (1993); (b) C. Bosshard, F. Pan, M. Wong, S. Mancetta, R. Spreiter, C. Cai, P. Günter, V. Gramlich. *Chem. Phys.*, **245**, 377 (1999); (c) J. Zyss (Ed.). *Molecular Nonlinear Optics: Material Physics and Devices*, Chap. 4, Academic Press Inc., San Diego (1993); (d) H. Nalwa, T. Watanabe, S. Miyata. *Nonlinear Optics of Organic Molecules and Polymers*, H. Nalwa, S. Miyata (Eds.), p. 89, CRC Press, Boca Raton (1997); (e) B. Coe. *Acc. Chem. Rev.*, **39**, 383 (2006); (f) B. Ivanova, M. Spiteller. *J. Phys. Chem. A*, **114**, 5099 (2010); (g) B. Ivanova, M. Spiteller. *Cryst. Growth Des.*, **10**, 2470 (2010); (h) B. Ivanova, M. Spiteller. *Struct. Chem.*, **21**, 989 (2010); (i) B. Ivanova, M. Spiteller. *Polyhedron*, **30**, 241 (2010); (j) S. Marder, J. Perry, W. Schaefer. *Science*, **245**, 626 (1989); (k) J. Wolff, R. Wortmann. *Adv. Phys. Org. Chem.*, **32**, 121 (1999); (l) S. Leininger, B. Olenyuk, P. Stang. *Chem. Rev.*, **100**, 853 (2000).

[9] (a) K. Siebert, K. Löffler, H. Quast, M. Thomson, T. Bauer, R. Leonhardt, S. Czasch, H. Roskos. *Phys. Med. Biol.*, **47**, 3743 (2002); (b) P. Siegel. *IEEE Trans. Microwave Theory Tech.*, **50**, 910 (2002); (c) C. Jansen, S. Wietzke, O. Peters, M. Scheller, N. Vieweg, M. Salhi, M. Krumbholz, C. Jördens, T. Hochrein, M. Koch. *Appl. Optics*, **49**, E48 (2005); (d) M. Theuer, R. Beigang, D. Grischkowsky. *Appl. Phys. Lett.*, **96**, 191110 (2010); (e) K. Oppenheim, T. Korter, J. Melinger, D. Grischkowsky. *J. Phys. Chem. A*, **114**, 12513 (2010); (f) S. Harsha, D. Grischkowsky. *J. Phys. Chem. A*, **114**, 3489 (2010).

[10] (a) G.M. Sheldrick. *Acta Cryst.*, **D66**, 479 (2010); (b) R. Blessing. *Acta Cryst.*, **A51**, 33 (1995); (c) A. Spek. *J. Appl. Cryst.*, **36**, 7 (2003); (d) H. Gillier. *Bull. Soc. Chim. Fr.*, 2373 (1965). *International Tables for X-ray Crystallography*, Vol. III, pp. 202–207, Kynoch Press, Birmingham (1962).

[11] (a) G. Olah, J. Flood. *J. Am. Chem. Soc.*, **84**, 1688 (1962); (b) E. Wilson. *J. Chem. Phys.*, **36**, 2232 (1962); (c) P. Politzer. *Chemical Applications of Atomic and Molecular Potentials*, P. Politzer, D.Truhlar (Eds.), Plenum Press, New York (1981); (d) J. Autschbach, F. Jorge, T. Ziegler. *Inorg. Chem.*, **42**, 2867 (2002); (e) Y. Zhao, D. Truhlar. *Acc. Chem. Res.*, **41**, 157 (2008); (f) M.J. Frisch, G.W. Trucks, H.B. Schlegel, G.E. Scuseria, M.A. Robb, J.R. Cheeseman, G. Scalmani, V. Barone, B. Mennucci, G.A. Petersson, H. Nakatsuji, M. Caricato, X. Li, H.P. Hratchian, A.F. Izmaylov, J. Bloino, G. Zheng, J.L. Sonnenberg, M. Hada, M. Ehara, K. Toyota, R. Fukuda, J. Hasegawa, M. Ishida, T. Nakajima, Y. Honda, O. Kitao, H. Nakai, T. Vreven, J.A. Montgomery Jr, J.E. Peralta, F. Ogliaro, M. Bearpark, J.J. Heyd, E. Brothers, K.N. Kudin, V.N. Staroverov, R. Kobayashi, J. Normand, K. Raghavachari, A. Rendell, J.C. Burant,

S.S. Iyengar, J. Tomasi, M. Cossi, N. Rega, J.M. Millam, M. Klene, J.E. Knox, J.B. Cross, V. Bakken, C. Adamo, J. Jaramillo, R. Gomperts, R.E. Stratmann, O. Yazyev, A.J. Austin, R. Cammi, C. Pomelli, J.W. Ochterski, R.L. Martin, K. Morokuma, V.G. Zakrzewski, G.A. Voth, P. Salvador, J.J. Dannenberg, S. Dapprich, A.D. Daniels, Ö. Farkas, J.B. Foresman, J.V. Ortiz, J. Cioslowski, D.J. Fox. *GausView03*, Gaussian, Inc., Wallingford, CT (2009); (g) *DALTON, A Molecular Electronic Structure Program*, Release Dalton2011 (2011). Available online at: http://daltonprogram.org/ (accessed 10 May 2012); (h) GausView03. Available online at: http://www.gaussian.com/g_prod/gv5_plat.htm (accessed 10 May 2012).; (i) F. Jensen. *Introduction to Computational Chemistry*, Wiley, New York (1999); (j) M. Head-Gordon, J. Pople, M. Frisch. *Chem. Phys. Lett*., **153**, 503 (1988); (k) B. Ivanova, M. Spiteller. *Biopolymers*, **39**, 727 (2010).

[12] (a) OpenOfficeOrg. Available online at: http://de.openoffice.org/ (accessed 10 May 2012). (b) C.T. Kelley. *Iterative Methods for Optimization*, Frontiers in Applied Mathematics, SIAM, Philadelphia (1999); (c) K. Madsen, H. Nielsen, O. Tingleff. *Informatics and Mathematical Modelling*, 2nd Edn, DTU Press, Lyngby (2004); (d) M. Lamshoft, B. Ivanova, M. Spiteller. *Talanta*, **85**, 2562 (2011); (e) B. Ivanova, M. Spiteller. *Biopolymers*, **97**, 134 (2912); (f) B. Ivanova, M. Spiteller. *Talanta*, **94**, 9 (2012); (g) B. Ivanova, M. Spiteller. *J. Pharm. Biomed. Anal.* (2012). doi.org/10.1016/j.jpba.2011.10.028 .

[13] (a) Y. Yang, J. Guan, P. Qiu, Q. Kan. *Trans. Met. Chem*., **35**, 263 (2010); (b) S. Dey, T. Mukherjee, S. Sarkar, H. Evans, P. Chattopadhyay. *Trans. Met. Chem*., DOI 10.1007/s11243-011-9512-0.

[14] (a) S. Oppenheimer, D. Mi, M. Sanders, R. Caprioli. *J. Proteome Res*., **9**, 2182 (2010); (b) R. Cole (Ed.), *Electrospray and MALDI Mass Spectrometry*, Wiley, New Jersey (2010).

[15] (a) R. Knochenmuss, F. Dubois, M. Dale, R. Zenobi. *Rapid Commun. Mass Spectrom*., **10**, 871 (1996); (b) M. Gimon, L. Preston, G. Kinsel, D. Russell. *Org. Mass Spectrom*., **27**, 827 (1992).

[16] (a) L. Preston-Schaffter, G. Kinsel, D. Russell. *J. Am. Soc. Mass Spectrom*., **5**, 800 (1994); (b) T. Constantopoulos, G. Jackson, C. Enke. *J. Am. Soc. Mass Spectrom*., **10**, 625 (1999); (c) C. Enke. *Anal. Chem*., **69**, 4885 (1997).